HHS Public Access

Author manuscript

Sci Signal. Author manuscript; available in PMC 2021 September 02.

Published in final edited form as:

Sci Signal. ; 14(672): . doi:10.1126/scisignal.aba2940.

A venous-specific purinergic signaling cascade initiated by Pannexin 1 regulates TNFα-induced increases in endothelial permeability

Daniela Maier-Begandt[1,2], **H Skye Comstra**[3], **Samuel A Molina**[3], **Nenja Krüger**[1,4], **Claire A Ruddiman**[1], **Yen Lin Chen**[1], **Xiaobin Chen**[1], **Lauren A Biwer**[1,5], **Scott R Johnstone**[6,7], **Alexander Lohman**[8,9], **Miranda E Good**[10], **Leon J DeLalio**[1], **Kwangseok Hong**[11], **Hannah Bacon**[1], **Zhen Yan**[1], **Swapnil K Sonkusare**[1,5], **Michael Koval**[3,12,*], **Brant E Isakson**[1,5,*]

[1]Robert M. Berne Cardiovascular Research Center, University of Virginia, School of Medicine, Charlottesville, VA 22908, US

[2]Walter Brendel Center of Experimental Medicine, University Hospital, and Institute of Cardiovascular Physiology and Pathophysiology, Biomedical Center, LMU Munich, 82152 Planegg-Martinsried, Germany

[3]Division of Pulmonary, Allergy, Critical Care and Sleep Medicine, Department of Medicine, Emory University School of Medicine, Atlanta, GA 30322, US

[4]Institute of Animal Developmental and Molecular Biology, Heinrich Heine University Düsseldorf, Germany

[5]Department of Molecular Physiology and Biophysics, University of Virginia School of Medicine, Charlottesville, VA 22908, US

[6]Fralin Biomedical Research Institute at Virginia Tech Carilion Center for Heart and Reparative Medicine Research, Virginia Tech, Roanoke VA 24016

[7]Department of Biological Sciences, Virginia Tech, Blacksburg VA 24060

[8]Hotchkiss Brain Institute, University of Calgary, Calgary, Alberta, T2N 4N1, Canada

[9]Department of Cell Biology and Anatomy, University of Calgary, Calgary, Alberta, T2N 4N1, Canada

[*]Corresponding Authors: Brant E. Isakson, PhD, Robert M. Berne Cardiovascular Research Center, Department of Molecular Physiology and Biophysics, University of Virginia School of Medicine, P.O. Box 801394, Charlottesville, VA 22908 USA, brant@virginia.edu; Michael Koval, PhD, Emory University School of Medicine, Division of Pulmonary, Allergy, Critical Care and Sleep Medicine, 205 Whitehead Building, 615 Michael Street, Atlanta, GA 30322, mhkoval@emory.edu.

Author contributions

DMB performed permeability assays. DMB, SAM, and MK created and analyzed data from Ussing chambers. NK, HB, MEG, LJD, LAB, AL, BEI, and SRJ utilized endothelial cells and performed mRNA analysis and western blots. AL and MK analyzed microarray data. YLC, KH, and SKS performed and analyzed calcium data. DMB, HB, SRJ, HSC, and CAR performed imaging. XC and ZY performed and analyzed sepsis experiments. DMB, SAM, MK, all BEI all participated in experimental design. DMB, MK, and BEI wrote and edited the manuscript. BEI and MK managed the project and financial backing.

Competing interests

The authors declare that they have no competing interests.

Data and materials availability

The microarray data has been deposited in the NCBI Gene Expression Omnibus and are accessible through GEO Series accession number GSE137041. All other data needed to evaluate the conclusions in the paper are present in the paper or the Supplementary Materials.

[10]Molecular Cardiology Research Institute, Tufts Medical Center, Boston, MA 02111, US

[11]Department of Physical Education, College of Education, Chung-Ang University, Seoul, 06974, South Korea

[12]Department of Cell Biology, Emory University School of Medicine, Atlanta, GA 30322, US

Abstract

The endothelial cell barrier regulates the passage of fluid between the bloodstream and underlying tissues, and barrier function impairment exacerbates the severity of inflammatory insults. To understand how inflammation alters vessel permeability, we studied the effects of the proinflammatory cytokine TNFα on transendothelial permeability and electrophysiology in ex vivo murine veins and arteries. We found that TNFα specifically decreased the barrier function of venous endothelium without affecting that of arterial endothelium. Based on RNA expression profiling and protein analysis, we found that CLDN11 was the predominant claudin in venous endothelial cells and that there was little, if any, CLDN11 in arterial endothelial cells. Consistent with a difference in claudin composition, TNFα increased the permselectivity of Cl^- over Na^+ in venous but not arterial endothelium. The vein-specific effects of TNFα also required the activation of Pannexin 1 (Panx1) channels and the CD39-mediated hydrolysis of ATP to adenosine which subsequently stimulated A_{2A} adenosine receptors. Moreover, the increase in vein permeability required the activation of the Ca^{2+} channel TRPV4 downstream of Panx1 activation. Panx1-deficient mice resisted the pathologic effects of sepsis induced by cecal ligation and puncture on lifespan and lung vascular permeability. These data provide a targetable pathway with the potential to promote vein barrier function and prevent the deleterious effects of vascular leak in response to inflammation.

Introduction

Under normal physiological conditions, the endothelial barrier of blood vessels maintains homeostasis by regulating the passage of water, ions and proteins between the blood and underlying tissues. Dysregulation or breakdown of the endothelial barrier is associated with pathophysiological conditions including stroke, hypertension, and sepsis (1-4). There are several proposed mechanisms by which endothelial barrier function becomes compromised, but there are few mechanistic studies using intact vessels and transgenic mouse models have been underutilized in this capacity.

The vascular tree has considerable diversity, with discrete regions having different physiologic characteristics and permeability (5). In the microcirculation, it is generally appreciated that, at baseline, veins are considerably more permeable to solutes than arteries and also have lower vessel electrical resistance (6, 7). In addition, it has been known for decades that capillaries and veins are substantially more sensitive than arteries to stimuli that induce vascular leakage, such as histamine (8), platelet-activating factor (9) and TNFα (10-12). However, the molecular mechanisms that confer increased sensitivity of veins over arteries to these agents have not been determined.

TNFα regulates inflammation in part by activating the endothelium, leading to leukocyte recruitment, transmigration and, ultimately, resolution of tissue inflammation at sites of injury or infection (13-15). TNFα activates Pannexin 1 (Panx1) channels on endothelial cells during inflammation by a Src family kinase (SFK)-mediated pathway to release ATP, a leukocyte attractant and activator (16, 17). Consistent with a role for Panx1 in inflammation, these channels have been implicated in ischemia/reperfusion injury in the brain (18), kidney (19) and lung (20) microvasculature. Ischemia/reperfusion injury is frequently associated with edema (20), suggesting that Panx1 may have a role in regulating vascular barrier function. However, Panx1 is central to the recruitment of immune cells to sites of injury (16, 17) which, in turn, can damage the endothelium. Because in vivo analysis is confounded by the immune response, it has not been determined whether Panx1 has a direct mechanistic role in regulating endothelial barrier function in response to pro-inflammatory cytokines.

Here we used ex vivo preparations of veins and arteries from various transgenic mouse models, as well as cultured primary human endothelial cells, to define roles for Panx1 in TNFα-induced disruption of endothelial barrier function. We found that barrier function of venous endothelial cells was significantly more sensitive to TNFα than arteries and that the decrease in barrier function was due to stimulated Ca^{2+} influx through transient receptor potential vanilloid 4 (TRPV4) channels following Panx1 activation. Also, in comparison to arteries, veins were enriched for ectonucleoside triphosphate diphosphohydrolase 1 (CD39), a rate limiting enzyme in nucleotide hydrolysis (21, 22)] in the pathway hydrolyzing ATP to adenosine that, in concert with ecto 5'-nucleotidease (CD73), metabolized extracellular ATP released through Panx1 to adenosine, thus stimulating A_{2A} adenosine receptors. CD39 and A_{2A} were required for venous leak induced by TNFα. Moreover, we found that claudin-11 (CLDN11) was specifically expressed by venous endothelium and not by arterial endothelial cells. These data show that Panx1 has a direct role in regulating endothelial barrier function and identify downstream mediators that increase venous sensitivity to TNFα.

Results

Vein endothelial barrier function was more sensitive to TNFα than artery endothelial barrier function

To investigate the effects of TNFα on vessel permeability, we measured vessel preparations using custom-made cassettes for a dual-channel, self-contained Ussing chamber (Figure 1A-D), analogous to an approach we previously used to measure intestinal permeability in situ (23). The cassettes were equipped with a 750 x 1500 μm opening that is small enough to be covered with a longitudinally sectioned vessel (Figure 1C and 1D). We isolated second or third order mouse mesenteric veins and arteries, cut them longitudinally, and then treated the vessels with either vehicle control or 50 ng/ml TNFα for 30 minutes. Under these conditions TNFα did not damage endothelial cells (Figure S1B). Afterwards, the vessel was mounted by fully covering the opening of the custom-made chamber cassette (Figure 1D), which was sealed and placed into the Ussing Chamber, with the endothelial cell side oriented as the apical face.

In the presence of physiological Ringer's solution, transendothelial electrical resistance (TEER) was measured from either control or TNFα-treated mouse veins and arteries.

Control veins showed a ~2.4-fold decrease in TEER 30 min after TNFα treatment (Figure 1E). By contrast, arteries did not show a significant change in TEER between vehicle control and TNFα treatment. Consistent with the TEER measurements, short circuit currents (Isc) were specifically decreased in TNFα-treated veins as opposed to arteries, where Isc was essentially unchanged by exposure to TNFα (Figure 1F). Thus, vein barrier function was specifically altered by TNFα.

Ussing chambers allow detailed electrophysiological characterization of samples. To determine whether TNFα affected ion permeability in native blood vessels, we performed dilution potential measurements to calculate the relative permeability of Na^+ to Cl^- (24, 25). Untreated veins and arteries both showed comparable Na^+ and Cl^- permeability, where P_{Na}/P_{Cl} was nearly 1 (Figure 1G). However, TNFα treatment specifically increased venous Cl^- permeability, as reflected by a decrease in P_{Na}/P_{Cl}. To further confirm changes in vessel ion permselectivity due to TNFα, we also examined the effect of TNFα on vessel transendothelial potential when the current was clamped to 0 mAmp. TNFα induced a change in vein polarity from 1.3 mV under control conditions to −1.1 mV in normal Ringers buffer (Figure 1H). Vein potential showed a comparable TNFα-dependent change in polarity when aspartate was substituted for Cl^- or lysine was substituted for Na^+, suggesting that the effect of TNFα on transendothelial potential involved changes in both Na^+ and Cl^- permeability. Arteries did not show this effect, regardless of buffer composition. Thus, ex vivo Ussing analysis revealed a venous-specific effect of TNFα on paracellular ion channel homeostasis.

To determine whether the vein specific effects of TNFα were due to endothelial cell function, we examined primary human venous cells (human umbilical vein endothelial cells (HUVECs) and human saphenous vein endothelial cells (HSaVECs)) and arterial cells (human aortic endothelial cells (HAoECs) and human coronary arterial endothelial cells (HCoEC)) cultured on Transwell inserts and measured the effect of TNFα on TEER with an EVOM voltmeter. Consistent with our observations from intact vessels in the Ussing chamber (Figure 1, E to H), TNFα treatment induced a decrease in the TEER of HUVECs and HSaVECs that was not observed for either HAoECs or HCoECs (Figure 2A,B). These results suggest that venous endothelial cells may be more sensitive to the effects of the pro-inflammatory cytokine TNFα on TEER than arterial endothelial cells.

Given the differential sensitivity of venous vs arterial endothelial cells to TNFα, we used qRT-PCR to screen mRNA isolated from HUVECs, HSaVECs, HAoECs and HCoECs for differences in *claudin* (*CLDN*) gene expression, focusing on claudin-encoding genes expressed by vascular endothelium, namely *CLDN1, CLDN3, CLDN5, CLDN11 and CLDN12* (26-28). Of these claudins, *CLDN11* showed the greatest difference in expression when comparing vein to artery mRNA suggesting that *CLDN11* could be considered a marker for venous endothelium (Figure 2C,D). Because *CLDN5* is considered to be the most prominent claudin expressed by endothelial cells, it was surprising that *CLDN11* was expressed at a ~4 fold higher level compared to *CLDN5* by venous endothelial cells (Figure 2C,D).

Moreover, gene expression profiling comparing mRNA isolated from HUVECs, HSaVECs, HAoECs and HCoECs demonstrated that *CLDN11* was the most highly enriched mRNA when comparing venous endothelial cells with arterial endothelial cells (Figures 2E, S2, S3, Data File S1). We further analyzed Cldn11 expression at the protein level, in primary cultures of human endothelial cells (Figure 2F) and in murine en face (Figure 2G) and transverse (Figure S4A) preparations of third order mesenteric veins and arteries. Although Cldn5 was consistently expressed by both venous and arterial endothelium, Cldn11 was preferentially expressed by venous endothelium. Together, these data suggest that *CLDN11* mRNA and Cldn11 protein expression can be used as a marker to distinguish venous endothelium from arterial endothelium.

TNFα-induced changes in venous endothelial barrier function were regulated by TRPV4

TRPV4 channels regulate endothelial barrier function and can be activated by multiple stimuli (29-33). TRPV4 channels are also activated by TNFα in odontoblasts (34). Thus, we tested whether endothelial TRPV4 channels were activated by TNFα and, given the vein-specific increase in permeability in response to TNFα, whether TRPV4 channel activation was enhanced in veins as compared with arteries.

Initially, we performed Ca^{2+} imaging experiments by quantifying local Ca^{2+} influx, "Ca^{2+} sparklets", arising through distinct regions of the plasma membrane containing TRPV4 channels. Third-order mesenteric veins and arteries from C57BL/6 mice cut transversely in en face preparation were incubated with the Ca^{2+}-binding dye Fluo-4 AM and imaged using confocal microscopy (Fig. 3A). The TRPV4 agonist GSK1016790A was added to identify healthy tissue and regions of interest with activatable TRPV4 channels. We found that The addition of TNFα (10 ng/ml) produced an increase in Ca^{2+} sparklets over baseline in both veins and arteries, where the TNFα-induced activation of TRPV4 channels induced significantly higher sparklet activity in veins than in arteries (Figure 3B, 3C). Moreover, addition of the TRPV4 inhibitor GSK2193784 inhibited sparklets induced by TNFα, confirming that the Ca^{2+} influx was due to TRPV4 channel activity.

To link TRPV4 channel activity to the effects of TNFα on endothelial permeability ex vivo, we adapted a previously described approach to measure the permeability of the fluorescent tracer molecule fluorescein in dissected, cannulated murine mesenteric veins and arteries (35) (Figure 3D, E). TNFα significantly increased fluorescein permeability in veins as opposed to arteries, which were significantly less sensitive to TNFα (Figure 3F and Figure S1A). This result underscores that by two different measures in intact vessels, TEER (Figure 1E) and transvessel flux of a fluorescent tracer (Figure 3F and Supplemental Figure 1A), veins became leakier and were significantly more responsive to TNFα than arteries.

We then used this perfusion system to measure TNFα-induced permeability in mesenteric veins isolated from *Trpv4*$^{+/+}$ and *Trpv4*$^{-/-}$ mice. Unlike *Trpv4*$^{+/+}$ wild type (WT) mice, where addition of TNFα led to a significant increase in permeability, veins isolated from *Trpv4*$^{-/-}$ mice were resistant to TNFα and showed no increase in permeability (Figure 3G). Moreover, veins from WT C57BL/6 mice perfused with the TRPV4 agonist GSK1016790A also showed a significant increase in permeability. Together, these results confirm a role for TRPV4 channels downstream from TNFα in regulating venous endothelial barrier function.

TNFα-induced changes in venous endothelial barrier function were regulated by pannexin channels

We have previously shown that Panx1 channels are specifically activated by TNFα in the venous endothelium, leading to the extracellular release of ATP (16), leading to the hypothesis that TRPV4 activation was downstream of Panx1 in endothelial cells. To test this hypothesis, we used pharmacological inhibition and genetic ablation of Panx1. We previously established that spironolactone can act as an acute inhibitor of Panx1 in addition to being a mineralcorticoid receptor antagonist (36). Consistent with a role for Panx1 in activating TRPV4 in venous endothelial cells, addition of spironolactone to veins isolated from C57BL/6 mice significantly decreased the ability of TNFα to enhance Ca^{2+} sparklet activity (Figure 4A). To place Panx1 upstream in a TRPV4-dependent vein permeability pathway, we examined the effect of spironolactone on vein barrier function. Pharmacologic blockade of Panx1 protected veins from TNFα-induced barrier weakening (Figure 4B). Critically, TNFα-induced permeability to fluorescein in veins isolated from human donors was also inhibited by spironolactone treatment (Figure 4C). In addition, veins from an inducible, endothelial-specific Panx1 knockout mouse developed by our group (*Cdh5-CreER*$^{T2+}$*/Panx1*$^{fl/fl}$) (16) showed fewer TRPV4 Ca^{2+} sparklets (Figure 4D) and also were resistant to TNFα-induced increases in paracellular fluorescein permeability (Figure 4E). Spironolactone and genetic ablation provided two complementary methods demonstrating that Panx1 is upstream of TNFα increases in permeability and Ca^{2+} sparklet activity.

To further link TNFα and Panx1 to changes in barrier function, we examined the effects of TNFα on Cldn11. Veins treated with 50 ng/ml TNFα showed disrupted the localization of Cldn11 to endothelial tight junctions, as reflected by an increase in junctional discontinuities, an effect that was reversed by spironolactone (Fig. 4F-I). Moreover, TNFα treatment of veins from *Cdh5-CreER*$^{T2+}$*/Panx1*$^{fl/fl}$ mice had little effect on Cldn11 as opposed to WT veins (Figure 4F-I, Figure S4B). Together, these data demonstrate that TNFα-activated Panx1 channels initiate a TRPV4 signaling response that leads to an increase in venous permeability that is partially due to a decrease in tight junction-associated Cldn11.

Purinergic signaling mediated TNFα-induced impairment of venous endothelial barrier function

In response to TNFα, Panx1 releases ATP that plays a critical role as a signaling molecule in venous endothelial cells (16). We therefore measured ATP in perfusate released by veins from WT mice in response to TNFα (Figure 5A). Although there was detectable ATP in vein perfusates, 79.7 ± 3.6 % of the purinergic species detected were ATP metabolites, specifically ADP, AMP and adenosine. This finding suggested that ATP released by Panx1 was rapidly hydrolyzed by endothelial ectonucleotidases. Thus, we performed an immunohistological screen of cross-sections of mesenteric veins and arteries from C57BL/6 mice for two prominent ectonucleotideases implicated in inflammation, CD39 and CD73 (37) (Figure 5B). Cultured primary endothelial cells were also screened by real-time PCR (Figure 5C). We found that although CD73 was expressed in both arteries and veins, as well as primary human cultures of arterial and venous endothelial cells, veins and venous endothelial cells were enriched for CD39 expression as compared with arteries and arterial

endothelial cells (Figure 5B,C). Microarray analysis of human endothelial cells also demonstrated a significant enrichment of *ENTPD1* mRNA (which encodes CD39) by venous endothelial cells as compared with arterial endothelial cells (Figure 2E, S2).

Confirming a key role for CD39 in venous-specific ATP metabolism, TNFα-stimulated veins from *CD39*$^{-/-}$ mice showed ~3.7-fold more ATP present in the perfusate than WT controls (Figure 5A). Moreover, pretreatment of WT veins with the ecto-ATPase CD39 inhibitor ARL67156 or genetic ablation of *CD39* inhibited the ability of TNFα to increase venous leak (Figure 5D-E), further implicating CD39 as a downstream component required for the effects of Panx1 on venous barrier function.

After ATP has been enzymatically processed by CD39 and CD73, the free adenosine produced can bind and stimulate adenosine receptors at the apical cellular surface (38). We performed real-time PCR expression analysis to profile adenosine receptor expression and found that the predominant subtypes present in both primary human venous and arterial endothelial cells were A_{2A} (*ADORA2A*) and A_{2B} (*ADORA2B*) (Figure 6A). By contrast, the expression of genes encoding the A_1 and A_3 subtypes was undetectable. Differences in adenosine receptor transcript levels between venous and arterial cells were modest (Figure 6A). However, in cross-sections of mesenteric veins and arteries from WT C57BL/6 mice analyzed by immunohistochemistry, there was a more prominent A_{2A} signal present in the apical surface of venous endothelial cells as compared with arterial endothelium (Figure 6B), whereas A_{2B} was comparably distributed in both veins and arteries.

Because there was differential CD39 and A_{2A} expression between arteries and veins, we assessed whether adenosine receptors present in veins contributed to TNFα-induced permeability. WT mesenteric veins pretreated with either the A_{2A} antagonist SCH58261 or the A_{2A}/A_{2B} antagonist ZM241385 eliminated the TNFα-induced increase in permeability (Figure 6C). Moreover, veins from A_{2A}-deficient mice also were not sensitive to the effects of TNFα on permeability (Figure 6D). By contrast, direct stimulation of WT veins using the A_{2A} agonist CGS21680 caused an increase in vein permeability that was comparable to that of veins stimulated by TNFα (Figure 6C) further underscoring a role for A_{2A} in regulating vein permeability.

Panx1 as a target to reduce severity of sepsis

Sepsis is a life-threatening condition due to an uncontrolled infection leading to increased TNFα and venous permeability.(39) To identify roles for Panx1 in the response to sepsis, we compared the response of *Cdh5-CreER*$^{T2+}$*/Panx1*$^{fl/fl}$ to control mice that were injured using the cecal ligation and puncture (CLP) injury model. In contrast to control mice which showed little survival two days after CLP injury, mice with an endothelial cell-specific depletion of Panx1 were largely viable 5 days after CLP (Figure 7A). Comparable results were obtained using WT C57BL/6 mice treated with 40 mg/kg spironolactone, which showed a trend towards improved viability (Figure 7B). Using the lung wet/dry weight ratio as a measure of pulmonary edema, we found that *Cdh5-CreER*$^{T2+}$*/Panx1*$^{fl/fl}$ mice and mice treated with spironolactone had significantly lower edema in response to CLP than controls, consistent with a preservation of endothelial barrier function in Panx1-deficient mice and Panx1-inhibited mice (Figure 7C,D). There also was less renal injury in septic Panx1-

deficient mice or in mice treated with spironolactone, as assessed by blood urea nitrogen (Figure S5A,B); however, there was little effect on heart rate (Figure S5C,D).

Together, these data support a model in which the enhanced sensitivity of veins to TNFα-induced vessel leak is primarily due to differential expression of the ectonucleoside triphosphate diphosphohydrolase CD39 and A_{2A} adenosine receptors. This differential expression provides a pathway in which ATP released by Panx1 channels is hydrolyzed to adenosine that acts as either an autocrine or paracrine stimulus to decrease barrier function in a vein-specific manner (Figure 8).

Discussion

There are several lines of evidence linking Panx1 channels to inflammation (16-20). Among the pathologic consequences of inflammation are vascular leak and tissue edema, suggesting a role for Panx1 in regulating vascular barrier function. However, because Panx1 channels are broadly expressed by cells such as leukocytes and interstitial cells, in vivo studies are unable to assign a direct role for Panx1 in regulating endothelial barrier function. Here, we used perfused, isolated vessel preparations and cultured endothelial cells to demonstrate that Panx1 activation by TNFα initiates a cascade that preferentially increases the paracellular permeability of venous endothelial cells. Critically, dissected vessels cannulated onto glass micropipettes allow the investigation of venous permeability in living intact vessels under flow that maintain the complex structure of vessels, including endothelial cells, pericytes, the basal membrane that separates the two cell types and the glycocalyx that lines the apical surface of endothelial cells (40). At the same time, perfused vessels enabled us to define the Panx1-dependent pathways that promote vessel leakage by endothelial cells in a native context while avoiding the confounding effects of Panx1 channels expressed by other cells activated by inflammation.

The barrier function of capillaries and post-capillary veins is substantially more sensitive to TNFα than arteries in vivo (10-12). However, the preferential effect of TNFα on venous endothelium is not absolute. For instance, TNFα increases the permeability of bovine pulmonary arterial endothelial cells, although this requires at least 4 h of treatment with 20-100 ng/ml TNFα (41, 42). Bovine aortic endothelial cells also show increased leak following a 45 min TNFα treatment period (43). We therefore compared mesenteric venular and arteriolar leak following a 30 min treatment period to specifically examine differences in early responses to TNFα between these two classes of vessels. Using this protocol, we revealed that venous blood vessels were more sensitive to the pro-inflammatory stimulus TNFα than arterial vessels.

Based on transcriptional profiling of cultured human endothelial cells, we found that *CLDN11* is the most enriched gene by venous endothelial cells as compared with arterial endothelial cells. Cldn11 protein expression paralleled the pattern of mRNA expression, such as human venous endothelial cells and murine veins were enriched for Cldn11 as compared with comparable arterial endothelium. Although there are previous reports that Cldn11 is highly expressed by the microvasculature (26-28) and corpus cavernosum (44), we found that Cldn11 was specifically enriched in venous endothelial cells whereas arterial

endothelial cells are Cldn11-deficient. Considering that there are few markers to distinguish venous from arterial endothelial cells, these data suggest that Cldn11 expression is likely to be a useful marker to identify venous endothelial cells.

Enhanced Cldn11 expression by venous endothelial cells also has functional ramifications. At baseline, Cldn11 expressing venous endothelial cells have a higher dilution potential (Figure 1H) than arterial endothelial cells that lack Cldn11, suggesting that Cldn11 fine tunes resting endothelial cell paracellular ion permeability (45). Moreover, when veins were treated with TNFα (Figure 1E,G) there was both a decrease in net barrier function (as measured by TEER) and also a change in tight junction permselectivity such that anion permeability was increased to a greater extent than cation permeability. These TNFα-induced changes in permselectivity further underscore the effect of altered tight junction composition on venous barrier function due to decreased Cldn11 expression and assembly into tight junctions (Figure 4E-G).

Venous endothelial cells were more sensitive to the effects of TNFα-stimulated Panx1 channels and showed a decrease in barrier function as compared with arterial endothelium. Because Panx1 is ubiquitously expressed by most endothelial cells, our findings indicated that venous endothelial cells have unique elements downstream from Panx1 that are not shared with arterial endothelial cells. Specifically, we found that veins expressed more of the ectonucleoside CD39, which is the rate limiting enzyme required in conjunction with the ecto-5'-nucleotidase CD73 to fully hydrolyze ATP to adenosine (37). Also, the CD39 inhibitor ARL67156 or CD39 deficiency protected veins from TNFα-induced leak, further verifying a role for endothelial CD39 in this effect.

In addition to constitutive expression by venous endothelium, CD39 expression also increases in response to injurious stimuli such as endotoxin and hypoxia (46, 47). Thus, CD39 could potentially play a role in regulating permeability in vessels where it is not constitutively expressed at baseline, such as in arteries. Whether this is the case remains to be determined. Nonetheless, control of venous permeability by localized, constitutive expression of CD39 by veins is consistent with their physiological role as sites for leukocyte adhesion and extravasation.

Inflammation and injury is more severe when the CD39/CD73 complex is impaired and CD73-upregulating agents have been tested as a therapeutic target for patients with acute respiratory distress syndrome (48-51). A protective effect of CD39 (and CD73) is in apparent contrast with our finding that CD39 is required for TNFα to induce venous barrier leak. However, any increase in severity of inflammation in mice with a global CD39 deficiency is likely to accompany increased leukocyte adhesion to sites of vessel inflammation, because adenosine inhibits recruitment in response to pro-inflammatory stimuli (52, 53). Whether this is due to endothelial CD39 is not known, because platelets, neutrophils and other leukocytes also express CD39 (54). By contrast, ATP is a potent stimulus to recruit immune cells in response to inflammation (16). Because veins do not leak in response to ATP, this raises the possibility that ATP release may be an early event to attract immune cells to sites of damage that remain relatively intact until they are

subsequently rendered leaky by ATP hydrolysis to adenosine, which also releases immune cells from strong attachment to the endothelium (55, 56).

A_{2A} receptors were required for veins to be sensitive to TNFα, because vessels from A_{2A}-deficient mice remained intact and the effects of TNFα were antagonized by the A_2 receptor inhibitors SCH58261 and ZM241385. Consistent with a role for A_{2A} in vessel permeability, the A_{2A} agonist Lexiscan increases the permeability of human brain microvascular endothelial cells and also permeabilizes the blood brain barrier in mice, an effect that is diminished in $A_{2A}^{-/-}$ mice (57, 58). Human lung microvascular endothelial cells, which lack A_{2A} receptors, retain barrier function in response to adenosine, thus underscoring a role for A_{2A} receptors in endothelial leak (59).

Given the established role for TRPV4 channels in increasing endothelial cell barrier permeability (29, 30, 60), we examined the effects of TNFα on TRPV4 channels in venous endothelium. In fact, veins showed greater TRPV4 channel activation as compared with arteries in response to TNFα, consistent with our observations that veins were rendered more permeable by TNFα than arteries. Moreover, veins from TRPV4-deficient mice resisted the effects of TNFα on endothelial barrier function.

Sepsis is a life-threatening condition that currently lacks targeted therapeutic treatment and instead relies on antibiotics, fluid resuscitation and supportive care (61). Over 250,000 patients die of sepsis each year, largely as a result of septic shock (62). Here we found in transgenic mouse models that endothelial Panx1 played a key role in the severity of sepsis. Critically, spironolactone had a protective effect in CLP injured mice, suggesting that Panx1 is a potential therapeutic target in the treatment of sepsis. The venous-specific signaling pathway we have defined downstream from Panx1 provides additional targets that may provide improved therapeutic options in the management of sepsis.

Our study provides evidence that TRPV4 activation was downstream from Panx1, because TNFα activation of Ca^{2+} sparklets was diminished in vessels treated with spironolactone. Also, vessels deficient for endothelial Panx1 had a level of Ca^{2+} sparklet activity that was comparable to WT vessels treated with the TRPV4 antagonist GSK219. TRPV4 has the capacity to activate Panx1 channels (63-65). In these instances, it is likely that Panx1 is specifically activated by localized TRPV4 sparklets, because a sustained increase in cytosolic Ca^{2+} has no effect on Panx1 (66, 67). One intriguing possibility is that Panx1 and TRPV4 channels in a complex may form a feed-forward cycle that amplifies the effects of proinflammatory cytokines on venous endothelial cells, a notion supported by the ability of TRPV4 activation to induce TNFα release (68). If this is the case, then agents targeting the reciprocal activation of Panx1 and TRPV4 channels would have utility in preventing the deleterious effects of vascular leak that accompany inflammation.

Materials and Methods

Mice

All mice were on a C57BL/6J genetic background, male, 10–14 weeks of age, and were cared for under the provisions of the University of Virginia and Emory Animal Care and Use

Committees and followed the National Institute of Health guidelines for the care and use of laboratory animals. Mice were anaesthetized with carbon dioxide or isoflurane (2.5%) and sacrificed by cervical dislocation. The inducible, endothelial cell-specific Panx1 knockout mice using VE-cadherin (Cdh5) specific cre recombinase expression (*Cdh5-CreER*$^{T2+}$/*Panx1*$^{fl/fl}$) were generated as previously described (16). Panx1 deletion was induced specifically in the vascular endothelium by intraperitoneal injection of Tamoxifen (TMX, 1 mg in 0.1 ml peanut oil vehicle) for 10 consecutive days into *Cdh5-CreER*$^{T2+}$/*Panx1*$^{fl/fl}$ mice; vehicle injected mice served as controls.

CD39$^{-/-}$ mice (69), adenosine receptor subtype $A_{2A}{}^{-/-}$ mice (70, 71) and *TRPV4*$^{-/-}$ mice (31, 72) were generated as previously described.

Human vascular biopsies

Vessels from human adipose tissue biopsy samples were aseptically obtained from the gluteal region as supervised by Dr. Eugene Barrett at the University of Virginia outpatient clinic (Institutional Review Board approval 20408), following the Declaration of Helsinki Principles. For research purposes, biopsies were from non-obese adult patients ranging in age from 40-60 years old and that were not being treated with adrenergic blocking agents (66).

Electrophysiological vessel measurements

Second and third order veins and arteries were isolated from mouse mesenteric circulation in a Ringer's solution (140 mM NaCl, 2 mM $CaCl_2$, 1mM $MgCl_2$, 10 mM glucose, 10 mM HEPES, pH 7.3). Veins or arteries 2-3 mm in length were dissected, the adventitia removed and cut longitudinally. The vessels were treated for 30 min at 37°C with 50 ng/ml TNFα (R&D Systems, recombinant murine or human TNFα was used accordingly) or control vehicle (0.1% DMSO in PBS) in a rotary incubator.

Tissues were oriented in custom-made cassettes (Department of Physics, Emory University) designed to fit a dual-channel, self-contained Ussing chamber (U2500, Warner Instruments) with the endothelial layer positioned facing the apical compartment. Cut, positioned veins were sealed in the cassettes with vacuum grease and a parafilm gasket, placed in the U2500, then equilibrated with Ringer's solution at 37°C using a temperature-controlled water bath. Solutions were bubbled with a 5% CO_2/95% O_2 medical-grade gas mixture to maintain oxygenation and pH. Ussing chamber data were collected with a VCC MC-8 Multichannel Voltage/Current Clamp controller and analyzed using Acquire & Analyze Software (Physiological Instruments) (23).

For transendothelial dilution potential measurements, veins were equilibrated in either Ringer's saline, Ringer's lysine (140 mM lysine-HCl, 2 mM $CaCl_2$, 1mM $MgCl_2$, 10 mM glucose, 10 mM HEPES, pH 7.3) or Ringer's aspartate (140 mM Na-aspartate, 2 mM $CaCl_2$, 1mM $MgCl_2$, 10 mM glucose, 10 mM HEPES, pH 7.3). Next, medium on the apical side of the Ussing chamber was replaced with an osmotically balanced 1:3 dilution (diluted with iso-osmolar mannitol solution: 280 mM mannitol, 2 mM $CaCl_2$, 1 mM $MgCl_2$, 10 mM glucose, 10 mM HEPES, pH 7.3) and equilibrated for 5 minutes in each solution. The measurements were performed when current was clamped to 0 Amp with voltage measured

in millivolts (24, 73). Tissue resistance and voltage measurements were made in Ringer's solution and calculated in Ohms*cm^2. The ratio of Na permeability to Cl permeability (P_{Na}/P_{Cl}) was calculated by the method of Hou et al. (74). All measurements were area corrected.

Ex vivo vessel dye permeability measurements

Ex vivo permeability assays were developed from *ex vivo* perfusion assay as previously described (16). Second and third order veins or arteries were isolated from mouse mesenteric circulation in a Krebs solution containing 118.4 mM NaCl, 4.7 mM KCl, 1.2 mM $MgSO_4$, 4 mM $NaHCO_3$, 1.2 mM KH_2PO_4, 10 mM HEPES, 6 mM glucose and 2 mM $CaCl_2$. Veins and arteries with 2-3 mm in length were dissected, the adventitia removed, cannulated onto glass micropipettes and sealed with sutures. In order to apply a constant flow to the lumen of the blood vessels, the micropipettes were connected to a perfusion pump system with a 3-way stopcock enabling different media or agents to be perfused through the vessel using Krebs solution supplemented with 1% BSA (Krebs/BSA). Prior to permeability measurements, cannulated vessels were equilibrated for 20 min with Krebs/BSA.

To assess vessel permeability, 10 μg/mL fluorescein (Sigma Aldrich, MW 376.27) in Krebs/BSA (Krebs/BSA/fluorescein) was perfused through the lumen of the vessel and diffusion into the abluminal compartment (containing Krebs/BSA) was collected at time intervals and measured. Quantification of fluorescein fluorescence (excitation 490 nm, emission 514 nm) of the collected abluminal fractions was carried out with a FLUOstar Omega microplate reader (BMG Labtech). Initially, non-treated, equilibrated vessels were measured for 30 min to obtain a baseline permeability measurement, then the abluminal buffer was supplemented with control vehicle (0.1% BSA in PBS) or 50 ng/ml TNFα for additional 30 min, with abluminal buffer collected for fluorometric analysis.

Vessel permeability (Perm) was defined as the ratio of the rate of dye flux from the vessel lumen into the abluminal side under experimental conditions divided by the rate of flux at baseline (Perm = $F/F_{baseline}$). TNFα-induced increases in permeability are presented as relative fluorescent units (RFU). To test the effects of different agents on permeability, vessels were treated during both baseline measurement (first 30 min incubation) and TNFα treatment or control conditions (second 30 min incubation). These agents included a Panx1 inhibitor (spironolactone, Sigma-Aldrich), an ecto-nucleotidase inhibitor (ARL67156, Tocris Bioscience), A_{2A} and A_2 receptor antagonists (SCH58261 and ZM241385, respectively, Tocris Bioscience). Agonists, including A_{2A} receptor agonist (CGS21680, Tocris Bioscience) and TRPV4 channel agonist (GSK1016790A (GSK101), Tocris Bioscience), were applied during the second 30 min incubation instead of TNFα. Vessels treated with different agents were compared to vehicle treated controls (0.1% DMSO).

Ca^{2+} imaging and analysis of TRPV4 Ca^{2+} sparklets

Third-order mesenteric vessel were isolated from C57BL/6 mice, cut transversely and pinned down on a SYLGARD block in *en face* preparation as previously described (31, 75). Vessels were incubated with fluo-4 AM (10 μM) at 30 °C for 30 min. All the experiments were performed at 37°C in bicarbonate physiological salt solution. Vessels were incubated

with cyclopiazonic acid (CPA, 20 μM) at 37°C for 15 min to deplete internal Ca^{2+} stores and then with a low level of the TRPV4 agonist GSK101 (6 nM) for 5 min to confirm a healthy endothelium and to detect sites where sparklets will occur. To determine the effect of TNFα on TRPV4 sparklets, TNFα (10 ng/ml) was applied for 5 min in the presence or absence of spironolactone (80 μM). Vessels were then treated with the TRPV4 inhibitor GSK2193784 (GSK219, 100 nM) for 10 min to confirm that the TNFα-induced increase in sparklets was due to TRPV4 channels.

Ca^{2+} signals were detected in a 1.7 μm^2 regions of interest and using an increase in fluorescence over the averaged image obtained from 10 images, where TRPV4 Ca^{2+} sparklets were measured as previously described (31, 75). The average TRPV4 channel activity is defined as NP_O (where N is the number of TRPV4 channels per site and P_O is the open state probability of the channel). NP_O was calculated using the Single Channel Search module of Clampfit, quantal amplitudes derived from all-points histograms ($\Delta F/F_0$ of 0.29 for fluo-4-loaded vessels), and the following equation: $NP_O = (T_{level1} + 2T_{level2} + 3T_{level3} + 4T_{level4}) / T_{total}$, where T represents the dwell time at each quantal level and T_{total} is the total recording duration. Average NP_O per site was obtained by averaging the NP_O for all the sites in a field. When a signal crossed the threshold and came back to the baseline, it was counted as one event. All the events in a field during the recording duration were combined to obtain total number of events per field of view. All the sites in a field of view during the recording duration were combined to obtain total number of sites per field where the fold change in sparklet activity was normalized to untreated baseline values.

Immunohistochemical staining

For immunohistochemical staining of transverse sections, C57BL/6 mice were euthanized with carbon dioxide and sacrificed by cervical dislocation followed by perfusion through the heart with 4% PFA in PBS for fixation. Mouse mesenteric tissue isolates containing second order artery and vein pairs were isolated and fixed in 4% PFA for 30 min, then incubated in 70% ethanol and subjected to paraffin embedding, sectioning (4–5 μm in thickness) and mounted on slides. For immunohistochemistry, sections on slides were deparaffinized and processed as previously described (16).

To analyze CD39 and CD73 expression, vessel sections were incubated with monoclonal antibodies directed against murine CD39 (clone EPR3678(2), Abcam) or CD73 (clone D7F9A, New England Biolabs), respectively. Expression of A_{2A} and A_{2B} adenosine receptors in cells of artery/vein pairs was determined with polyclonal antibodies directed against murine A_{2A} (Thermo PA1-042) or A_{2B} (Thermo PA5-33322) respectively. Antibody specificity was confirmed by secondary antibody only control or by exchange of primary antibodies with the appropriate IgG control antibody.

For immunohistochemical staining of vessels *en face*, freshly isolated second or third order mesenteric arteries and veins were fixed with either 4% paraformaldehyde at 4°C for 30 min (CLDN5, Thermofisher, 34-1600), or with a 1:1 methanol acetone mixture at RT for 10 minutes (CLDN11, Abcam, ab53041). In some cases, vessels were treated *ex vivo* with TNFα (10ng/ml in Krebs/BSA) for 30 min at RT in the presence or absence of spironolactone pretreatment (10 μM in Krebs/BSA) for 15 min at RT before fixation.

Following PBS washes, vessels were cut *en face* and pinned out with tungsten wire (0.013 mm diameter) on Sylgard. Next, *en face* preparations were permeabilized in 0.2% NP40/PBS at RT for 30 minutes, incubated in 5% goat serum at RT for 1 hour (in 0.2% NP40/PBS), and incubated with primary antibody at 4°C overnight (1:100 in 5% serum/ 0.2% NP40/PBS). The next day *en face* preparations were washed in PBS and incubated with a secondary antibody (Thermofisher, A21069) at RT for 1 hour (1:400 in 5% goat serum/0.2% NP40/PBS). Following PBS washes, they were mounted on microscope slides with DAPI mounting media; images were obtained using an Olympus Fluoview 1000 microscope.

To quantify the effect of TNFα on tight junction morphology, images were thresholded using ImageJ and scored for areas of cell-cell contact lacking CLDN11 that were 5 μm or greater in length as a junctional discontinuity. For each preparation, three fields of view containing at least 8 endothelial cells were scored using vein preparations from at least three different mice.

Measurement of Adenosine metabolites

Vessels were perfused with Krebs/BSA solution for 30 min. The perfusate was collected and diluted to a final proportion of 1:1 inhibitor solution in Krebs/BSA containing 6 mM EDTA, 10 μM EHNA (Sigma-Aldrich), 40 μM dipyridamole (Sigma-Aldrich), 5 nM NBTI, 10 μM forskolin (Sigma-Aldrich), 100 μM IBMX (Calbiochem), 10 μM EHNA (Sigma-Aldrich), and 10 μM ITU (Sigma-Aldrich) (76). To extract metabolites, 1 ml of perfusate was diluted with 4 ml methanol, acetone, and acetonitrile (1:1:1) and the resulting supernatant was analyzed by LC-MS and compared with calibration standards. Individual adenosine containing metabolites were normalized to the total of ATP + ADP + AMP + adenosine present in the sample.

Cell culture

Primary human umbilical vein endothelial cells (HUVEC) were purchased from Cell Applications (200K-05), primary human saphenous vein endothelial cells (HSaVEC) and human aortic endothelial cells (HAoEC) from PromoCell (C-12231 and C-12271, respectively) and human coronary arterial endothelial cells (HCoEC) from Lonza (CC-2585). All cells were cultured in Microvascular Endothelial Cell Growth Medium-2 (complete medium, EGM-2MV, Lonza) and used for no more than 5 passages (16).

In vitro measurement of transendothelial electrical resistance

For *in vitro* transendothelial electrical resistance (TEER) measurements, cells were seeded on a fibronectin (Sigma Aldrich, 25 μg/ml)-coated Transwell polycarbonate membrane (6.5 mm diameter, 3.0 μm pore size, Corning Costar) at 1×10^5 cells per well (100 μl apical volume), in a 24-well plate tissue culture dish containing 600 μl of medium (abluminal compartment). After 24 h of culture, cells were used for TEER experiments. At 30 min prior to TEER measurements TNFα (10 and 100 ng/ml, respectively, R&D Systems) or vehicle (0.1% BSA in PBS, control) was added to the cells in the upper compartment. Subsequently, cells were placed in an EndOhm chamber (World Precision Instruments) and TEER was

measured using the Millicell-ERS (Electrical Resistance System, Millipore). A Transwell chamber without cells was used as a blank.

Quantitative real-time PCR and microarray analysis

RNA was isolated from HUVEC, HAOEC, HSaVEC and HCEC using the RNeasy mini kit (Qiagen, Cat.-No.: 74104) with respective DNase digestion (RNase free DNase set, Qiagen, Cat.-No.: 79254). The isolated RNA was then revered transcribed into cDNA using random hexamers and SuperScript III (ThermoFisher, Cat.-No. 18080093). To analyze transcript expression, cDNA was used as a template for real-time PCR analysis using the TaqMan Gene Expression Master Mix (ThermoFisher, Cat.-No. 4369016). Each transcript was measured in duplicates using gene-specific TaqMan probes and the relative transcript expression was determined compared to housekeeping gene B2M by using the X0 method (77). Target TaqMan probes used were CD39 Hs00969559_m1; CD73 Hs00159686_m1; ADORA 2A Hs00169123_m1; ADORA 2B Hs00386497_m1; ADORA 1 Hs00379752_m1; ADORA 3 Hs00252933_m1; B2M Hs00984230_m1

For microarray analysis, cytoplasmic RNA was isolated as described above and analyzed on an Agilent 2100 Bioanalyzer (Agilent, Palo Alto, CA) to assess RNA integrity. Double-stranded cDNAs were synthesized from total RNA by using the cDNA Synthesis System (Invitrogen, Carlsbad, CA). Biotin-labeled cRNA was generated and used to probe Affymetrix HuGene 1.0 ST v1 Arrays according to the manufacturer's recommendations (Expression Analysis Technical Manual, 2001, Affymetrix, Santa Clara, CA). For each Affymetrix dataset, raw celfiles were normalized using invariant set normalization and the PM-MM model of expression was used to construct gene expression measures and standard errors for each probe set (dCHIP). An N=3 for each cell type allowed for weighted mean and variance calculations. Probe sets in the top 5% with a fold difference greater than +/− 2.0 were analyzed. Probe sets with an absolute difference less than 100 expression units relative to control were removed for all Affymetrix array analyses. This filtering allowed for identification of genes well above background levels. Absent calls were also excluded. Microarray data was analyzed using Transcriptome Analysis Console (TAC) Software (Applied Biosystems, ThermoFisher Scientific) to produce expression scatterplots and for hierarchical cluster analysis. Microarray data were uploaded onto the NIH Gene Expression Omnibus (GEO) website, accession # GSE137041.

Sepsis model

Mice were subjected to the cecal ligation and puncture (CLP) model of peritonitis-induced sepsis (78). Mice were anesthetized using isoflurane, and then a midline abdominal incision was made, and the cecum was ligated immediately distal to the ileocecal valve. The cecum was then punctured with an 18-gauge needle, a small amount of stool was extruded and the gut was returned to the abdominal cavity which was closed in layers. All septic mice were injected subcutaneously with 1 ml of normal saline to balance fluid losses that occurred during surgery. For functional analysis, mice received antibiotics (ceftriaxone 25 mg/kg + metronidazole 12.5 mg/kg, intraperitoneally) at 3 and 15 hours postoperatively and then were euthanized 24 h after CLP. Mice that were followed for 5 days for survival studies received antibiotics at 48h.

Statistics

All graphs and statistics were produced or calculated using GraphPad Prism. Unpaired Two-Tailed T-Tests, One-way, and Two-way ANOVA tests were used to determine statistical significance as specified in the figure legends. RT-PCR data was analyzed for statistical significance by One-way ANOVA followed by Tukey's post hoc test. Results are presented as mean ± SD or mean ± SEM as indicated in the figure legends.

Supplementary Material

Refer to Web version on PubMed Central for supplementary material.

Acknowledgments

$A_{2A}^{-/-}$ mice were a kind gift of Victor E. Laubach (University of Virginia School of Medicine). We thank the Emory Department of Physics machine shop for design and fabrication of custom cassettes for the Ussing chamber.

Funding

This work was supported by R01-HL137112 (BEI, MK), R01-AA025854 (MK), R01-HL120840 (BEI), R56-HL138496 (SKS), R00- HL143165 (MEG), K12-GM000680 (HSC), AHA-CDA 19CDA34630036 (SRJ), DFG SFB914 A02 (DMB) and DFG IRTG 1902 (NAK).

References and Notes

1. Rosenberg GA, Neurological diseases in relation to the blood-brain barrier. J Cereb Blood Flow Metab 32, 1139–1151 (2012). [PubMed: 22252235]
2. Schoknecht K, Shalev H, Blood-brain barrier dysfunction in brain diseases: clinical experience. Epilepsia 53 Suppl 6, 7–13 (2012).
3. Granger DN, Rodrigues SF, Yildirim A, Senchenkova EY, Microvascular responses to cardiovascular risk factors. Microcirculation 17, 192–205 (2010). [PubMed: 20374483]
4. Wang Y, Gu Y, Granger DN, Roberts JM, Alexander JS, Endothelial junctional protein redistribution and increased monolayer permeability in human umbilical vein endothelial cells isolated during preeclampsia. Am J Obstet Gynecol 186, 214–220 (2002). [PubMed: 11854638]
5. Hilfenhaus G, Nguyen DP, Freshman J, Prajapati D, Ma F, Song D, Ziyad S, Cuadrado M, Pellegrini M, Bustelo XR, Iruela-Arispe ML, Vav3-induced cytoskeletal dynamics contribute to heterotypic properties of endothelial barriers. The Journal of cell biology 217, 2813–2830 (2018). [PubMed: 29858212]
6. Duran WN, Sanchez FA, Breslin JW, in Handbook of Physiology: Microcirculation Tuma RF, Duran WN, Ley K, Eds. (Academic Press, San Diego, CA, 2008), pp. 81–124.
7. Crone C, Christensen O, Electrical resistance of a capillary endothelium. J Gen Physiol 77, 349–371 (1981). [PubMed: 7241087]
8. Majno G, Palade GE, Schoefl GI, Studies on inflammation. II. The site of action of histamine and serotonin along the vascular tree: a topographic study. The Journal of biophysical and biochemical cytology 11, 607–626 (1961). [PubMed: 14468625]
9. Dillon PK, Duran WN, Effect of platelet-activating factor on microvascular permselectivity: dose-response relations and pathways of action in the hamster cheek pouch microcirculation. Circulation research 62, 732–740 (1988). [PubMed: 2450695]
10. Skinner RA, Tucker VL, Curry FR, Acute effects of tumor necrosis factor on hydraulic conductivity of mammalian postcapillary venules. The Journal of trauma 47, 486–491 (1999). [PubMed: 10498302]
11. Matsuki T, Beach JM, Klindt RL, Duling BR, Modification of vascular reactivity by alteration of intimal permeability: effect of TNF-alpha. The American journal of physiology 264, H1847–1853 (1993). [PubMed: 8322913]

12. Wong RK, Baldwin AL, Heimark RL, Cadherin-5 redistribution at sites of TNF-alpha and IFN-gamma-induced permeability in mesenteric venules. The American journal of physiology 276, H736–748 (1999). [PubMed: 9950877]
13. Ley K, Laudanna C, Cybulsky MI, Nourshargh S, Getting to the site of inflammation: the leukocyte adhesion cascade updated. Nature reviews. Immunology 7, 678–689 (2007).
14. Muller WA, Transendothelial migration: unifying principles from the endothelial perspective. Immunological reviews 273, 61–75 (2016). [PubMed: 27558328]
15. Alon R, van Buul JD, Leukocyte Breaching of Endothelial Barriers: The Actin Link. Trends Immunol 38, 606–615 (2017). [PubMed: 28559148]
16. Lohman AW, Leskov IL, Butcher JT, Johnstone SR, Stokes TA, Begandt D, DeLalio LJ, Best AK, Penuela S, Leitinger N, Ravichandran KS, Stokes KY, Isakson BE, Pannexin 1 channels regulate leukocyte emigration through the venous endothelium during acute inflammation. Nat Commun 6, 7965 (2015). [PubMed: 26242575]
17. Chen Y, Corriden R, Inoue Y, Yip L, Hashiguchi N, Zinkernagel A, Nizet V, Insel PA, Junger WG, ATP release guides neutrophil chemotaxis via P2Y2 and A3 receptors. Science 314, 1792–1795 (2006). [PubMed: 17170310]
18. Good ME, Eucker SA, Li J, Bacon HM, Lang SM, Butcher JT, Johnson TJ, Gaykema RP, Patel MK, Zuo Z, Isakson BE, Endothelial cell Pannexin1 modulates severity of ischemic stroke by regulating cerebral inflammation and myogenic tone. JCI insight 3, (2018).
19. Jankowski J, Perry HM, Medina CB, Huang L, Yao J, Bajwa A, Lorenz UM, Rosin DL, Ravichandran KS, Isakson BE, Okusa MD, Epithelial and Endothelial Pannexin1 Channels Mediate AKI. Journal of the American Society of Nephrology : JASN 29, 1887–1899 (2018). [PubMed: 29866797]
20. Sharma AK, Charles EJ, Zhao Y, Narahari AK, Baderdinni PK, Good ME, Lorenz UM, Kron IL, Bayliss DA, Ravichandran KS, Isakson BE, Laubach VE, Pannexin-1 channels on endothelial cells mediate vascular inflammation during lung ischemia-reperfusion injury. American journal of physiology 315, L301–L312 (2018). [PubMed: 29745255]
21. Borg N, Alter C, Gorldt N, Jacoby C, Ding Z, Steckel B, Quast C, Bonner F, Friebe D, Temme S, Flogel U, Schrader J, CD73 on T Cells Orchestrates Cardiac Wound Healing After Myocardial Infarction by Purinergic Metabolic Reprogramming. Circulation 136, 297–313 (2017). [PubMed: 28432149]
22. Yu JC, Lin G, Field JJ, Linden J, Induction of antiinflammatory purinergic signaling in activated human iNKT cells. JCI Insight 3, (2018).
23. Laukoetter MG, Nava P, Lee WY, Severson EA, Capaldo CT, Babbin BA, Williams IR, Koval M, Peatman E, Campbell JA, Dermody TS, Nusrat A, Parkos CA, JAM-A regulates permeability and inflammation in the intestine in vivo. The Journal of experimental medicine 204, 3067–3076 (2007). [PubMed: 18039951]
24. Koval M, Ward C, Findley MK, Roser-Page S, Helms MN, Roman J, Extracellular Matrix Influences Alveolar Epithelial Claudin Expression and Barrier Function. Am J Respir Cell Mol Biol 42, 172–180 (2010). [PubMed: 19423774]
25. Uhlig S, Yang Y, Waade J, Wittenberg C, Babendreyer A, Kuebler WM, Differential regulation of lung endothelial permeability in vitro and in situ. Cellular physiology and biochemistry : international journal of experimental cellular physiology, biochemistry, and pharmacology 34, 1–19 (2014).
26. Uchida Y, Sumiya T, Tachikawa M, Yamakawa T, Murata S, Yagi Y, Sato K, Stephan A, Ito K, Ohtsuki S, Couraud PO, Suzuki T, Terasaki T, Involvement of Claudin-11 in Disruption of Blood-Brain, -Spinal Cord, and -Arachnoid Barriers in Multiple Sclerosis. Molecular neurobiology 56, 2039–2056 (2019). [PubMed: 29984400]
27. Cording J, Berg J, Kading N, Bellmann C, Tscheik C, Westphal JK, Milatz S, Gunzel D, Wolburg H, Piontek J, Huber O, Blasig IE, In tight junctions, claudins regulate the interactions between occludin, tricellulin and marvelD3, which, inversely, modulate claudin oligomerization. Journal of cell science 126, 554–564 (2013). [PubMed: 23203797]
28. Berndt P, Winkler L, Cording J, Breitkreuz-Korff O, Rex A, Dithmer S, Rausch V, Blasig R, Richter M, Sporbert A, Wolburg H, Blasig IE, Haseloff RF, Tight junction proteins at the blood-

brain barrier: far more than claudin-5. Cell Mol Life Sci 76, 1987–2002 (2019). [PubMed: 30734065]

29. Wu S, Jian MY, Xu YC, Zhou C, Al-Mehdi AB, Liedtke W, Shin HS, Townsley MI, Ca2+ entry via alpha1G and TRPV4 channels differentially regulates surface expression of P-selectin and barrier integrity in pulmonary capillary endothelium. American journal of physiology 297, L650–657 (2009). [PubMed: 19617313]
30. Alvarez DF, King JA, Weber D, Addison E, Liedtke W, Townsley MI, Transient receptor potential vanilloid 4-mediated disruption of the alveolar septal barrier: a novel mechanism of acute lung injury. Circulation research 99, 988–995 (2006). [PubMed: 17008604]
31. Sonkusare SK, Bonev AD, Ledoux J, Liedtke W, Kotlikoff MI, Heppner TJ, Hill-Eubanks DC, Nelson MT, Elementary Ca2+ signals through endothelial TRPV4 channels regulate vascular function. Science 336, 597–601 (2012). [PubMed: 22556255]
32. Matsumoto K, Yamaba R, Inoue K, Utsumi D, Tsukahara T, Amagase K, Tominaga M, Kato S, Transient receptor potential vanilloid 4 channel regulates vascular endothelial permeability during colonic inflammation in dextran sulphate sodium-induced murine colitis. Br J Pharmacol 175, 84–99 (2018). [PubMed: 29053877]
33. Yin J, Hoffmann J, Kaestle SM, Neye N, Wang L, Baeurle J, Liedtke W, Wu S, Kuppe H, Pries AR, Kuebler WM, Negative-feedback loop attenuates hydrostatic lung edema via a cGMP-dependent regulation of transient receptor potential vanilloid 4. Circulation research 102, 966–974 (2008). [PubMed: 18323527]
34. El Karim I, McCrudden MT, Linden GJ, Abdullah H, Curtis TM, McGahon M, About I, Irwin C, Lundy FT, TNF-alpha-induced p38MAPK activation regulates TRPA1 and TRPV4 activity in odontoblast-like cells. Am J Pathol 185, 2994–3002 (2015). [PubMed: 26358221]
35. Yuan Y, Chilian WM, Granger HJ, Zawieja DC, Permeability to albumin in isolated coronary venules. The American journal of physiology 265, H543–552 (1993). [PubMed: 8368358]
36. Good ME, Chiu YH, Poon IKH, Medina CB, Butcher JT, Mendu SK, DeLalio LJ, Lohman AW, Leitinger N, Barrett E, Lorenz UM, Desai BN, Jaffe IZ, Bayliss DA, Isakson BE, Ravichandran KS, Pannexin 1 Channels as an Unexpected New Target of the Anti-Hypertensive Drug Spironolactone. Circulation research 122, 606–615 (2018). [PubMed: 29237722]
37. Antonioli L, Pacher P, Vizi ES, Hasko G, CD39 and CD73 in immunity and inflammation. Trends in molecular medicine 19, 355–367 (2013). [PubMed: 23601906]
38. Johnston-Cox HA, Koupenova M, Ravid K, A2 adenosine receptors and vascular pathologies. Arterioscler Thromb Vasc Biol 32, 870–878 (2012). [PubMed: 22423039]
39. Angus DC, van der Poll T, Severe sepsis and septic shock. N Engl J Med 369, 2063 (2013).
40. Rodrigues SF, Granger DN, Blood cells and endothelial barrier function. Tissue Barriers 3, e978720 (2015). [PubMed: 25838983]
41. Petrache I, Verin AD, Crow MT, Birukova A, Liu F, Garcia JG, Differential effect of MLC kinase in TNF-alpha-induced endothelial cell apoptosis and barrier dysfunction. American journal of physiology 280, L1168–1178 (2001). [PubMed: 11350795]
42. Petrache I, Birukova A, Ramirez SI, Garcia JG, Verin AD, The role of the microtubules in tumor necrosis factor-alpha-induced endothelial cell permeability. Am J Respir Cell Mol Biol 28, 574–581 (2003). [PubMed: 12707013]
43. Xu SQ, Mahadev K, Wu X, Fuchsel L, Donnelly S, Scalia RG, Goldstein BJ, Adiponectin protects against angiotensin II or tumor necrosis factor alpha-induced endothelial cell monolayer hyperpermeability: role of cAMP/PKA signaling. Arterioscler Thromb Vasc Biol 28, 899–905 (2008). [PubMed: 18292388]
44. Wessells H, Sullivan CJ, Tsubota Y, Engel KL, Kim B, Olson NE, Thorner D, Chitaley K, Transcriptional profiling of human cavernosal endothelial cells reveals distinctive cell adhesion phenotype and role for claudin 11 in vascular barrier function. Physiological genomics 39, 100–108 (2009). [PubMed: 19622796]
45. Van Itallie CM, Fanning AS, Anderson JM, Reversal of charge selectivity in cation or anion-selective epithelial lines by expression of different claudins. Am J Physiol Renal Physiol 285, F1078–1084 (2003). [PubMed: 13129853]

46. Eltzschig HK, Kohler D, Eckle T, Kong T, Robson SC, Colgan SP, Central role of Sp1-regulated CD39 in hypoxia/ischemia protection. Blood 113, 224–232 (2009). [PubMed: 18812468]
47. Kittel A, Lipopolysaccharide treatment modifies pH- and cation-dependent ecto-ATPase activity of endothelial cells. J Histochem Cytochem 47, 393–400 (1999). [PubMed: 10026241]
48. Koszalka P, Ozuyaman B, Huo Y, Zernecke A, Flogel U, Braun N, Buchheiser A, Decking UK, Smith ML, Sevigny J, Gear A, Weber AA, Molojavyi A, Ding Z, Weber C, Ley K, Zimmermann H, Godecke A, Schrader J, Targeted disruption of cd73/ecto-5'-nucleotidase alters thromboregulation and augments vascular inflammatory response. Circulation research 95, 814–821 (2004). [PubMed: 15358667]
49. Eckle T, Fullbier L, Wehrmann M, Khoury J, Mittelbronn M, Ibla J, Rosenberger P, Eltzschig HK, Identification of ectonucleotidases CD39 and CD73 in innate protection during acute lung injury. J Immunol 178, 8127–8137 (2007). [PubMed: 17548651]
50. Bellingan G, Brealey D, Mancebo J, Mercat A, Patroniti N, Pettila V, Quintel M, Vincent JL, Maksimow M, Jalkanen M, Piippo I, Ranieri VM, Comparison of the efficacy and safety of FP-1201-lyo (intravenously administered recombinant human interferon beta-1a) and placebo in the treatment of patients with moderate or severe acute respiratory distress syndrome: study protocol for a randomized controlled trial. Trials 18, 536 (2017). [PubMed: 29132404]
51. Yegutkin GG, Helenius M, Kaczmarek E, Burns N, Jalkanen S, Stenmark K, Gerasimovskaya EV, Chronic hypoxia impairs extracellular nucleotide metabolism and barrier function in pulmonary artery vasa vasorum endothelial cells. Angiogenesis 14, 503–513 (2011). [PubMed: 21922294]
52. Eltzschig HK, Thompson LF, Karhausen J, Cotta RJ, Ibla JC, Robson SC, Colgan SP, Endogenous adenosine produced during hypoxia attenuates neutrophil accumulation: coordination by extracellular nucleotide metabolism. Blood 104, 3986–3992 (2004). [PubMed: 15319286]
53. Dwyer KM, Deaglio S, Gao W, Friedman D, Strom TB, Robson SC, CD39 and control of cellular immune responses. Purinergic signalling 3, 171–180 (2007). [PubMed: 18404431]
54. Ziegler M, Hohmann JD, Searle AK, Abraham MK, Nandurkar HH, Wang X, Peter K, A single-chain antibody-CD39 fusion protein targeting activated platelets protects from cardiac ischaemia/reperfusion injury. Eur Heart J 39, 111–116 (2018). [PubMed: 28472483]
55. Wong CW, Christen T, Roth I, Chadjichristos CE, Derouette JP, Foglia BF, Chanson M, Goodenough DA, Kwak BR, Connexin37 protects against atherosclerosis by regulating monocyte adhesion. Nature medicine 12, 950–954 (2006).
56. Yuan D, Wang Q, Wu D, Yu M, Zhang S, Li L, Tao L, Harris AL, Monocyte-endothelial adhesion is modulated by Cx43-stimulated ATP release from monocytes. Biochemical and biophysical research communications 420, 536–541 (2012). [PubMed: 22446325]
57. Kim DG, Bynoe MS, A2A Adenosine Receptor Regulates the Human Blood-Brain Barrier Permeability. Molecular neurobiology 52, 664–678 (2015). [PubMed: 25262373]
58. Carman AJ, Mills JH, Krenz A, Kim DG, Bynoe MS, Adenosine receptor signaling modulates permeability of the blood-brain barrier. The Journal of neuroscience : the official journal of the Society for Neuroscience 31, 13272–13280 (2011). [PubMed: 21917810]
59. Batori R, Kumar S, Bordan Z, Cherian-Shaw M, Kovacs-Kasa A, MacDonald JA, Fulton DJR, Erdodi F, Verin AD, Differential mechanisms of adenosine- and ATPgammaS-induced microvascular endothelial barrier strengthening. Journal of cellular physiology 234, 5863–5879 (2019). [PubMed: 29271489]
60. Stevens T, Functional and molecular heterogeneity of pulmonary endothelial cells. Proceedings of the American Thoracic Society 8, 453–457 (2011). [PubMed: 22052919]
61. Rhodes A, Evans LE, Alhazzani W, Levy MM, Antonelli M, Ferrer R, Kumar A, Sevransky JE, Sprung CL, Nunnally ME, Rochwerg B, Rubenfeld GD, Angus DC, Annane D, Beale RJ, Bellinghan GJ, Bernard GR, Chiche JD, Coopersmith C, De Backer DP, French CJ, Fujishima S, Gerlach H, Hidalgo JL, Hollenberg SM, Jones AE, Karnad DR, Kleinpell RM, Koh Y, Lisboa TC, Machado FR, Marini JJ, Marshall JC, Mazuski JE, McIntyre LA, McLean AS, Mehta S, Moreno RP, Myburgh J, Navalesi P, Nishida O, Osborn TM, Perner A, Plunkett CM, Ranieri M, Schorr CA, Seckel MA, Seymour CW, Shieh L, Shukri KA, Simpson SQ, Singer M, Thompson BT, Townsend SR, Van der Poll T, Vincent JL, Wiersinga WJ, Zimmerman JL, Dellinger RP, Surviving Sepsis Campaign: International Guidelines for Management of Sepsis and Septic Shock: 2016. Intensive Care Med 43, 304–377 (2017). [PubMed: 28101605]

62. Gaieski DF, Edwards JM, Kallan MJ, Carr BG, Benchmarking the incidence and mortality of severe sepsis in the United States. Critical care medicine 41, 1167–1174 (2013). [PubMed: 23442987]
63. Rahman M, Sun R, Mukherjee S, Nilius B, Janssen LJ, TRPV4 Stimulation Releases ATP via Pannexin Channels in Human Pulmonary Fibroblasts. Am J Respir Cell Mol Biol 59, 87–95 (2018). [PubMed: 29393654]
64. Shahidullah M, Mandal A, Delamere NA, TRPV4 in porcine lens epithelium regulates hemichannel-mediated ATP release and Na-K-ATPase activity. Am J Physiol Cell Physiol 302, C1751–1761 (2012). [PubMed: 22492652]
65. Seminario-Vidal L, Okada SF, Sesma JI, Kreda SM, van Heusden CA, Zhu Y, Jones LC, O'Neal WK, Penuela S, Laird DW, Boucher RC, Lazarowski ER, Rho signaling regulates pannexin 1-mediated ATP release from airway epithelia. The Journal of biological chemistry 286, 26277–26286 (2011). [PubMed: 21606493]
66. DeLalio LJ, Billaud M, Ruddiman CA, Johnstone SR, Butcher JT, Wolpe AG, Jin X, Keller T. C. S. t., Keller AS, Riviere T, Good ME, Best AK, Lohman AW, Swayne LA, Penuela S, Thompson RJ, Lampe PD, Yeager MY, Isakson BE, Constitutive SRC-mediated phosphorylation of pannexin 1 at tyrosine 198 occurs at the plasma membrane. The Journal of biological chemistry, (2019).
67. Weilinger NL, Lohman AW, Rakai BD, Ma EM, Bialecki J, Maslieieva V, Rilea T, Bandet MV, Ikuta NT, Scott L, Colicos MA, Teskey GC, Winship IR, Thompson RJ, Metabotropic NMDA receptor signaling couples Src family kinases to pannexin-1 during excitotoxicity. Nature neuroscience 19, 432–442 (2016). [PubMed: 26854804]
68. Matsumoto K, Deguchi A, Motoyoshi A, Morita A, Maebashi U, Nakamoto T, Kawanishi S, Sueyoshi M, Nishimura K, Takata K, Tominaga M, Nakahara T, Kato S, Role of transient receptor potential vanilloid subtype 4 in the regulation of azoymethane/dextran sulphate sodium-induced colitis-associated cancer in mice. Eur J Pharmacol 867, 172853 (2020). [PubMed: 31836532]
69. Enjyoji K, Sevigny J, Lin Y, Frenette PS, Christie PD, Esch JS 2nd, Imai M, Edelberg JM, Rayburn H, Lech M, Beeler DL, Csizmadia E, Wagner DD, Robson SC, Rosenberg RD, Targeted disruption of cd39/ATP diphosphohydrolase results in disordered hemostasis and thromboregulation. Nature medicine 5, 1010–1017 (1999).
70. Sharma AK, Linden J, Kron IL, Laubach VE, Protection from pulmonary ischemia-reperfusion injury by adenosine A2A receptor activation. Respiratory research 10, 58 (2009). [PubMed: 19558673]
71. Lappas CM, Rieger JM, Linden J, A2A adenosine receptor induction inhibits IFN-gamma production in murine CD4+ T cells. J Immunol 174, 1073–1080 (2005). [PubMed: 15634932]
72. Liedtke W, Friedman JM, Abnormal osmotic regulation in trpv4−/− mice. Proceedings of the National Academy of Sciences of the United States of America 100, 13698–13703 (2003). [PubMed: 14581612]
73. Alexandre MD, Lu Q, Chen YH, Overexpression of claudin-7 decreases the paracellular Cl- conductance and increases the paracellular Na+ conductance in LLC-PK1 cells. Journal of cell science 118, 2683–2693 (2005). [PubMed: 15928046]
74. Hou J, Renigunta A, Gomes AS, Hou M, Paul DL, Waldegger S, Goodenough DA, Claudin-16 and claudin-19 interaction is required for their assembly into tight junctions and for renal reabsorption of magnesium. Proceedings of the National Academy of Sciences of the United States of America 106, 15350–15355 (2009). [PubMed: 19706394]
75. Hong K, Cope EL, DeLalio LJ, Marziano C, Isakson BE, Sonkusare SK, TRPV4 (Transient Receptor Potential Vanilloid 4) Channel-Dependent Negative Feedback Mechanism Regulates Gq Protein-Coupled Receptor-Induced Vasoconstriction. Arterioscler Thromb Vasc Biol 38, 542–554 (2018). [PubMed: 29301784]
76. Gorman MW, Feigl EO, Buffington CW, Human plasma ATP concentration. Clinical chemistry 53, 318–325 (2007). [PubMed: 17185366]
77. Thomsen R, Solvsten CA, Linnet TE, Blechingberg J, Nielsen AL, Analysis of qPCR data by converting exponentially related Ct values into linearly related X0 values. Journal of bioinformatics and computational biology 8, 885–900 (2010). [PubMed: 20981893]

78. Yoseph BP, Breed E, Overgaard CE, Ward CJ, Liang Z, Wagener ME, Lexcen DR, Lusczek ER, Beilman GJ, Burd EM, Farris AB, Guidot DM, Koval M, Ford ML, Coopersmith CM, Chronic alcohol ingestion increases mortality and organ injury in a murine model of septic peritonitis. PLoS One 8, e62792 (2013). [PubMed: 23717394]

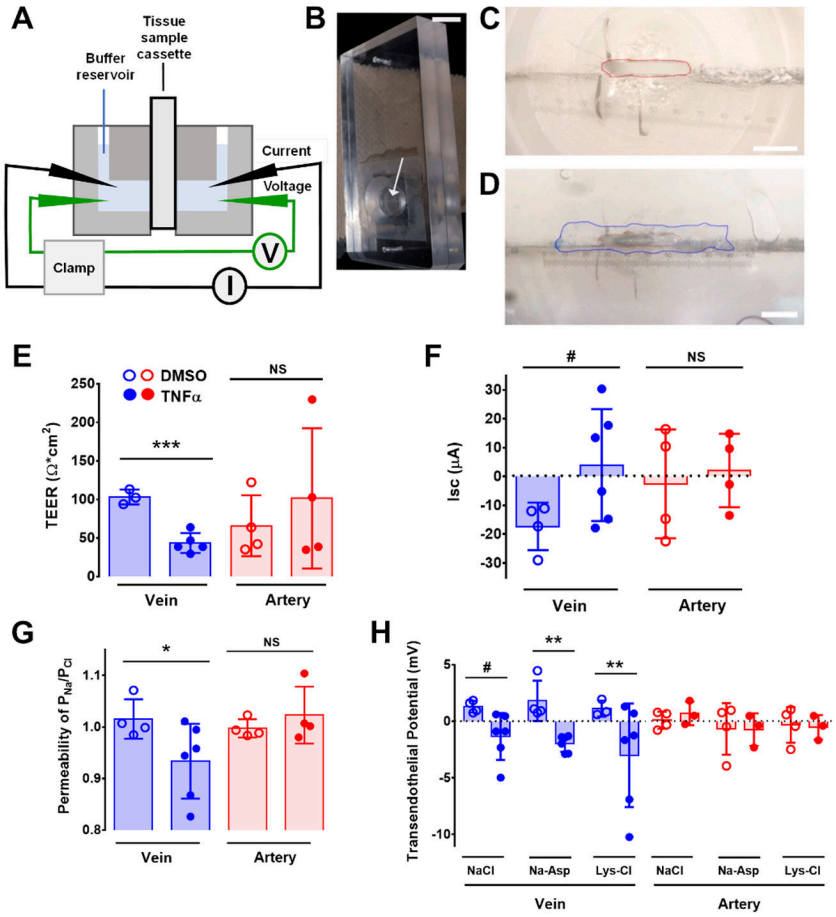

Figure 1. Custom Ussing system to measure electrophysiological characteristics of *ex vivo* mesenteric vessels.

(**A**) Schematic of a self-contained Ussing chamber system which can house two custom-made tissue cassettes. (**B**) Custom-made cassette for vessel analysis. The arrow indicates the horizontal opening of the cassette. Scale bar, 1 cm. (**C** and **D**) Magnified image of the cassette showing the opening with an approximate area of 0.26 mm^2 (red line, C), which can be completely covered with a longitudinally-sectioned vessel (border of the vein marked in blue, D). Scale bars, 750 μm (C) and 650 μm (D). (**E** – **G**) Ex vivo second and third order mesenteric arteries or veins of C57BL/6 mice were treated with vehicle (0.1% DMSO in PBS) or TNFα (50 ng/ml) for 30 minutes and mounted on Ussing chamber cassettes in physiologic Ringer's solution. TEER (E), short-circuit current (Isc) (F), and ion permeability (G) were measured. (**H**) Transendothelial dilution potential measurements in veins and arteries treated with TNFα in normal Ringer's solution or Ringer's where NaCl was exchanged with either 140 mM Na-Asp or Lys-HCl . *** $P = 0.0005$ (E); # $P = 0.076$ (F) by unpaired two-tailed t-test. * $P = 0.034$ by One-way ANOVA Fisher's LSD Test (G). # $P = 0.064$ and ** $P = 0.0093$ by Two-way ANOVA Fisher's LSD Test (H). n = 3-6 venules, n = 3-4 arterioles for each treatment representing biological replicates. Graphs represent mean ± SD.

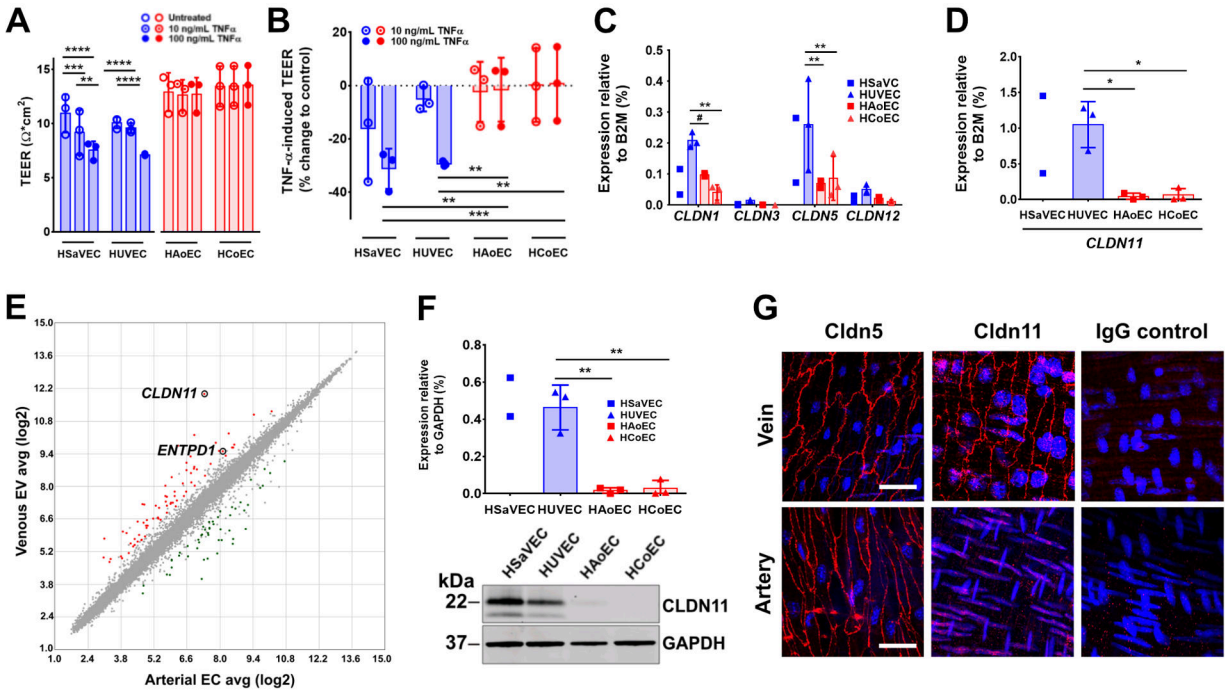

Figure 2. Effects of TNFα on barrier function and differential claudin expression by venous endothelium.

(**A, B**) TEER in Ω*cm^2 (A) or as % change (B) to control of untreated or TNFα-treated (10 and 100 ng/mL) human venous endothelial cells (HSaVEC, HUVEC) and human arterial endothelial cells (HAoEC, HCoEC) cultured on Transwell permeable supports (n = 3 different human donors). (**C**,**D**) Quantification of *CLDN1, CLDN3, CLDN5, CLDN12* (C), and *CLDN11* (D) gene expression by real-time PCR in human vein endothelial cells (HSaVEC, HUVEC) and human arterial endothelial cells (HAoEC, HCoEC) (n = 2 – 3 independent RNA preparations). (**E**) Scatterplot showing microarray transcription profiling analysis comparing venous endothelial cells (HSaVEC, HUVEC) with arterial endothelial cells (HAoEC, HCoEC). The tight junction protein gene *CLDN11* and *ENTPD1* (which encodes CD39) are highlighted. (**F**) Representative immunoblot (F) of CLDN11 expression in cell lysates from HSaVEC, HUVEC, HAoEC, and HCoEC. Protein expression of CLDN11 is normalized to the amount of GAPDH protein expression (100%) (n = 2 – 3 independent protein preparations). (**G**) Representative microscopic images of second order mesenteric veins and arteries from C57BL/6 mice presented en face immunostained for Cldn5, Cldn11 or IgG control for labeling specificity (red). Nuclei were stained with DAPI (blue). Scale bar, 100 μm. ** P = 0.0015, *** P = 0.0009, **** P < 0.0001 (A); ** P = 0.0012, 0.0017, 0.0011, *** P = 0.0008 (B); ** P = 0.0069, 0.0028, 0.0054, # P = 0.0673 (C); ** P = 0.0020, 0.0023 by Two-way ANOVA Fisher's LSD Test (F). * P = 0.034, 0.037 by One-way ANOVA Fisher's LSD Test (D). Graphs represent mean ± SD.

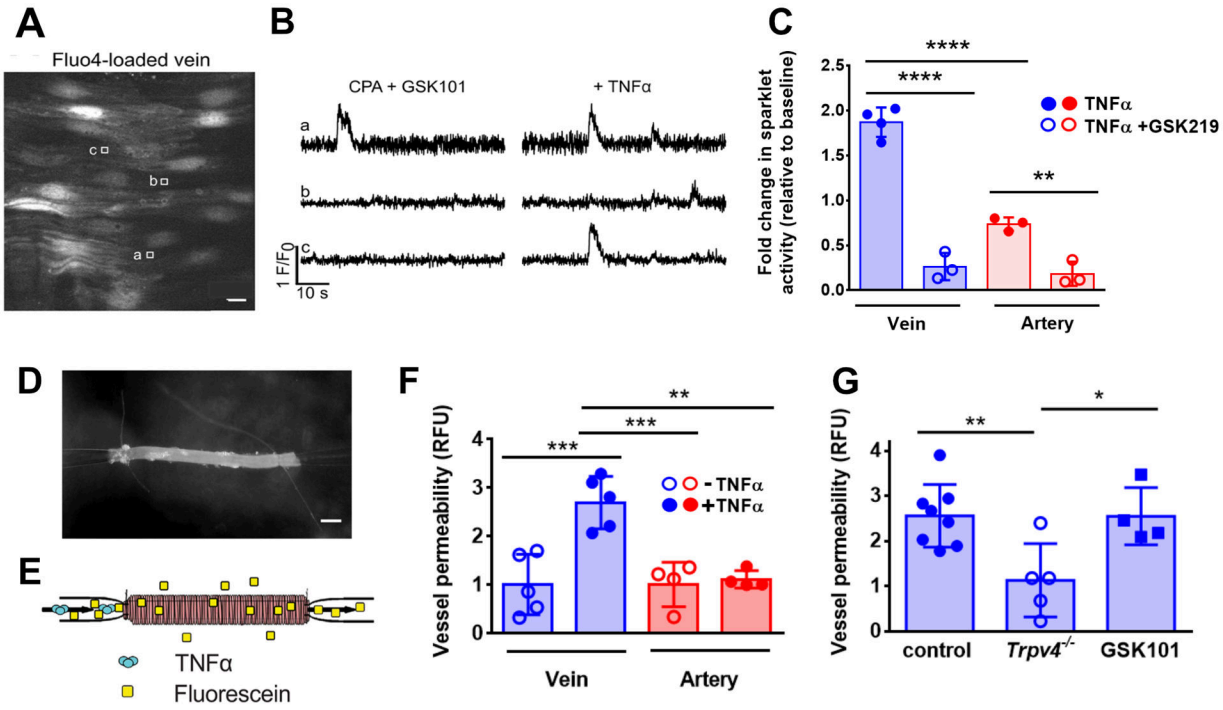

Figure 3. TNFα-stimulated venous barrier permeability required TRPV4.

(**A and B**) Representative greyscale image of Fluo-4-loaded, en face mesenteric vein of C57BL/6 mice (A). Scale bar, 10 μm. Square boxes (a,b,c) indicate regions of interest placed at Ca^{2+} sparklet sites to record fractional fluorescence (F/F_0) traces (B). Experiments were performed in the presence of cyclopiazonic acid (CPA, 20 μM) to eliminate Ca^{2+} release from the endoplasmic reticulum and also in the presence of the TRPV4 channel agonist GSK1016790A (GSK101, 6nM). (**C**) Ca^{2+} sparklet activity was recorded before and after stimulation with TNFα (10 ng/mL). TNFα-induced sparklet activity in the absence or presence of the TRPV4 inhibitor GSK2193784 (GSK219) was quantified ($n = 5$ vessels for each treatment). (**D**) Image of a vein cannulated and sutured onto glass micropipettes for ex vivo analysis. Scale bar, 100 μm. (**E**) Schematic of the perfusion system, to measure vessel permeability ex vivo, adapted from (16). Vessels were perfused through the lumen with 10 μg/ml fluorescein in Krebs/0.1% BSA containing 50 ng/ml TNFα and permeability was measured. (**F**) Permeability induced by TNFα in venous ($n = 5$) and arterial ($n = 4$) mesenteric vessels vessels from C57BL/6 mice. (**G**) Permeability induced by TNFα (10 ng/mL) in veins from *Trpv4*$^{+/+}$ mice (control) or from *Trpv4*$^{-/-}$ mice ($n = 5$-8 veins for each genotype) or veins from C57BL/6 mice treated with the TRPV4 agonist GSK1016790A (GSK101; 100 nM) ($n = 4$ veins). ** $P = 0.0040$, **** $P < 0.0001$ (C); ** $P = 0.0015$, *** $P = 0.0005$, 0.0009 (F); * $P = 0.027$, ** $P = 0.0097$ (G) by One-way ANOVA with Tukey's multiple comparisons test. Graphs represent mean ± SD.

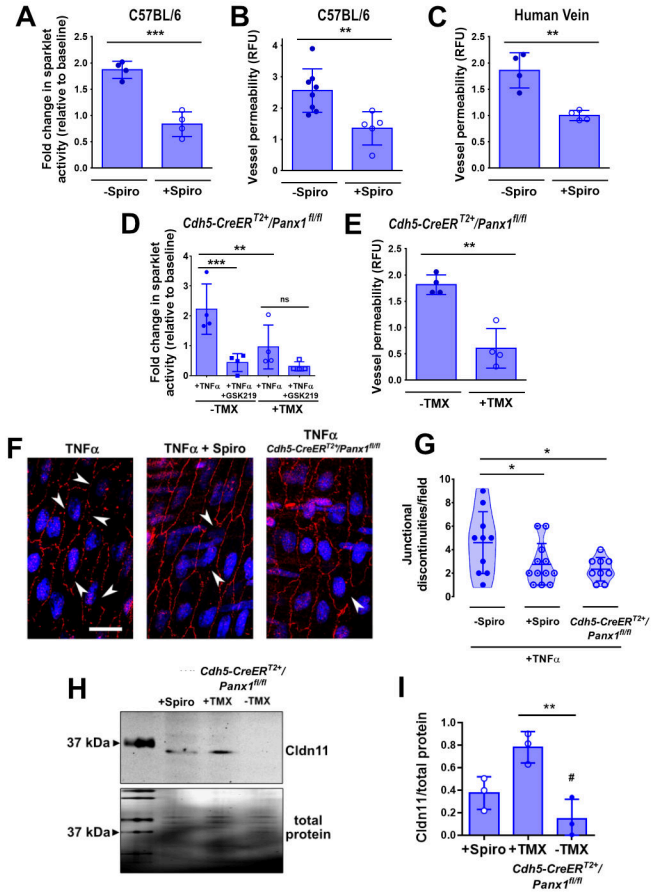

Figure 4. TNFα-stimulated venous barrier permeability required Panx1.

(**A**) Effect of spironolactone (Spiro, 80 μM) on TRPV4 sparklets induced by TNFα (10 ng/mL) in en face mesenteric veins of C57BL/6 mice (n = 4 veins for each treatment). (**B,C**) Effect of spironolactone (Spiro, 80 μM) on TNFα-induced permeability of veins from C57BL/6 mice (B) or from human adipose tissue biopsy samples (C) (n = 5 veins for each treatment). (**D**) Effect of the TRPV4 inhibitor GSK2193784 (GSK219) on TRPV4 sparklets induced by TNFα (10 ng/mL) in second order mesenteric veins from *Cdh5-CreER^{T2+}/Panx1$^{fl/fl}$* mice injected with tamoxifen (+TMX) to induce Panx1 deficiency or veins from control mice (−TMX) (n = 4 veins for each treatment). (**E**) TNFα-induced permeability of mesenteric veins from *Cdh5-CreER^{T2+}/Panx1$^{fl/fl}$* mice injected with tamoxifen (+TMX) or veins isolated from mice treated with vehicle control alone (−TMX, n = 4 veins for each treatment). (**F,G**) Representative microscopic images of TNFα-treated (10 ng/mL), en face second order mesenteric veins either pretreated with spironolactone (15 min, Spiro, 10 μM) from C57BL/6 mice or from *Cdh5-CreER^{T2+}/Panx1$^{fl/fl}$* mice injected with tamoxifen. Cldn11 was immunostained with a specific antibody (red) and nuclei were stained with DAPI (blue). The amount of Cldn11 localized to endothelial tight junctions was measured by the presence of junctional discontinuities (G). Scale bar, 100 μm. n = 3-4 fields imaged of vessel preparations from 3 mice for each treatment (**H, I**) Representative immunoblot (H) and quantitative analysis (I) of whole cell lysates of either spironolactone-pretreated and TNFα-treated (10 ng/mL) second order mesenteric veins from C57BL/6 mice or of second

order mesenteric veins from *Cdh5-CreER*$^{T2+}$/*Panx1*$^{fl/fl}$ mice injected with tamoxifen or vehicle control and treated with TNFα (10 ng/mL). Total protein expression was used as loading control. $n = 3$ protein isolates from biological replicates. *** $P = 0.0004$ (A); ** $P = 0.0071$ (B); ** $P = 0.0026$ (C); ** $P = 0.0012$ (E) by unpaired two-tailed t-test. *** $P = 0.001$, ** $P = 0.0097$ (D); * P = 0.0336, 0.0165 (G); ** $P = 0.0054$, # $P = 0.119$ (vs +Spiro) (I) by One-way ANOVA with Fisher's LSD test. Graphs represent mean ± SD.

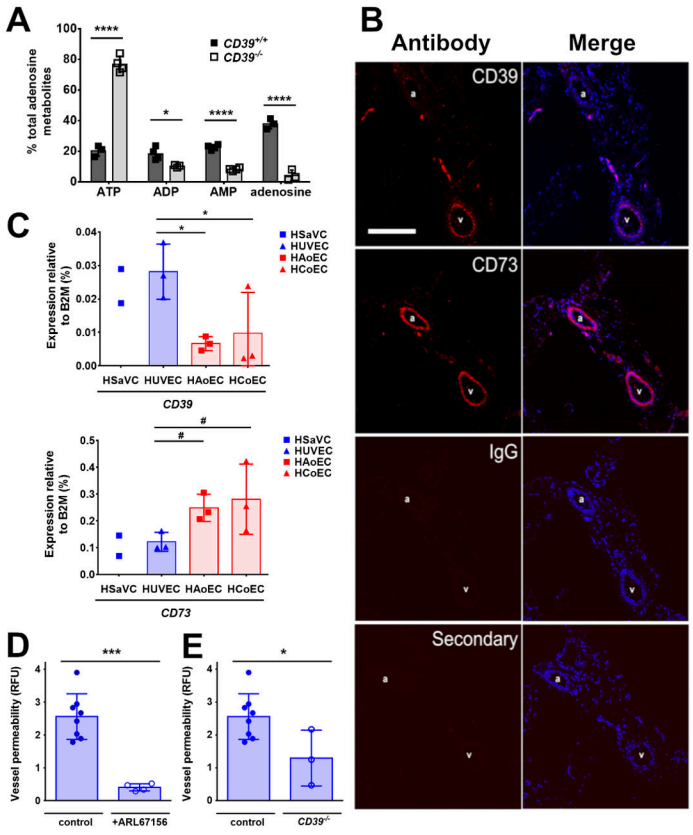

Figure 5. Venous endothelial cells expressed higher amounts of the ecto-nucleoside CD39 than arterial endothelial cells.

(A) Veins were isolated from *CD39*$^{+/+}$ and *CD39*$^{-/-}$ mice, incubated with TNFα (10 ng/mL) and adenosine metabolites were measured ($n = 3$ independent vessel perfusates per group). (**B**) Representative images from immunohistochemical staining of CD39 and CD73 using specific antibodies to label mesenteric artery (a) and vein (v) pairs in sections from C57BL/6 mice. Labeling specificity was determined by IgG and secondary only controls. CD73 and CD39 are labeled with secondary antibodies (red), nuclei are stained with DAPI (blue). Scale bar, 100 μm. (**C**) Expression analysis of ecto-nucleoside triphosphate diphosphohydrolase (*ENTPD1; CD39*) (upper panel), and ecto-5′-nucleotidase (*NT5E; CD73)* (lower panel) by real-time PCR in human vein endothelial cells (HSaVEC, HUVEC) and human arterial endothelial cells (HAoEC, HCoEC) compared with the housekeeping gene *B2M* ($n = 2$-3 different human donors). (**D, E**) TNFα-induced permeability was measured in veins from C57BL/6 mice in the presence of the CD39 antagonist ARL67156 (300 μM, $n = 4$ veins) (D) or in veins from *CD39*$^{-/-}$ mice ($n = 3$ veins) (E). * $P = 0.018$, ****, $P < 0.0001$ by two-way ANOVA with Sidak's multiple comparisons test (A), * $P = 0.022, 0.040$, # $P = 0.1131, 0.0587$ by one-way ANOVA with Fisher's LSD test (C). *** $P = 0.0001$ (D), * $P = 0.32$ (E) by unpaired two-tailed t-test (D-E). Graphs are mean ± SD.

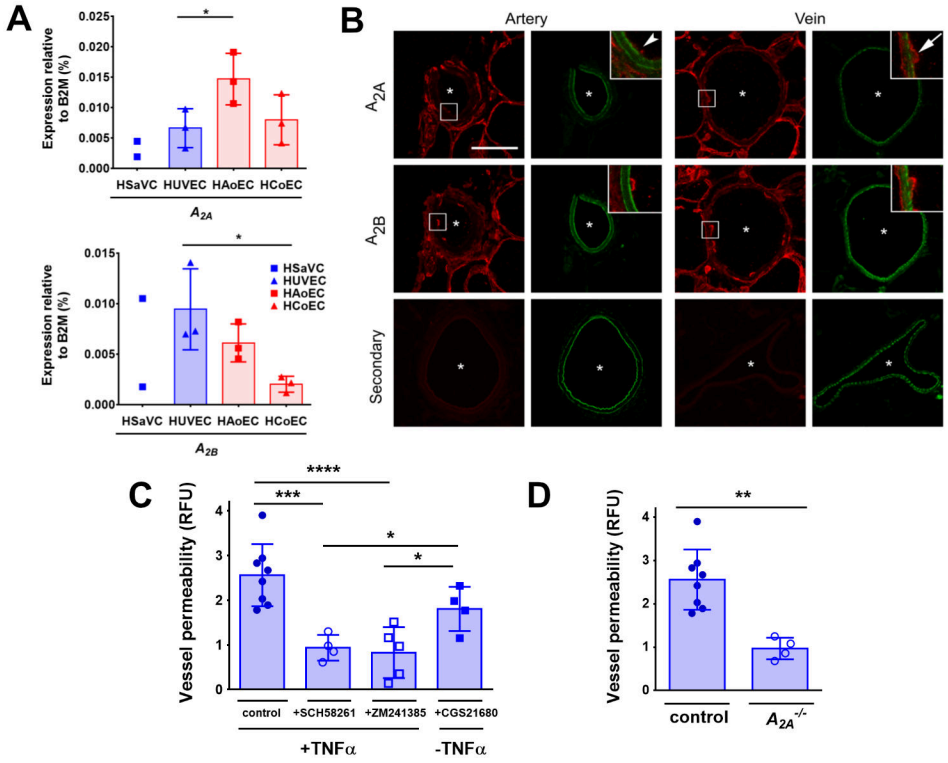

Figure 6. A_{2A} receptors were required for TNFα-stimulated increases in venous endothelial permeability.

(**A**) Expression analysis of adenosine receptors A_{2A} (*ADORA2A*) and A_{2B} (*ADORA2B*) by real-time PCR in human venous endothelial cells (HSaVEC, HUVEC) and human arterial endothelial cells (HAoEC, HCoEC) as compared to housekeeping gene *B2M* (n = 2-3 different human donors). (**B**) Representative images of immunohistochemical labeling of A_{2A} and A_{2B} in mesenteric sections from C57BL/6 mice containing arteries or veins. Asterisks indicate vessel lumens. A_{2A} and A_{2B} were labeled with a secondary antibody (red), and vessels were marked by autofluorescence of the internal elastic lamina (IEL) (green). Representative examples of n = 3 independent experiments. Scale bar, 50 μm. (**C**) TNFα-induced permeability was measured in veins of C57BL/6 mice pre-treated with either the A_{2A} antagonist SCH58261 (100 nM, n = 4 independent vessel preparations), A_{2A}/A_{2B} antagonist ZM241385 (100 nM, n = 5 independent vessel preparations) or treated with the A_{2A} agonist CGS21680 (100 nM) in the absence of TNFα (n = 4 independent vessel preparations. (**D**) TNFα-induced permeability was measured in veins from $A_{2A}^{+/+}$ (control) or $A_{2A}^{-/-}$ mice (n = 4 independent vessel preparations). * P = 0.042, 0.013 (A); *** P = 0.0003, * P = 0.048, 0.022, **** P < 0.0001 (C) one-way ANOVA with Fisher's LSD test. ** P = 0.0015 by unpaired two-tailed t-test (D). Graphs are mean ± SD.

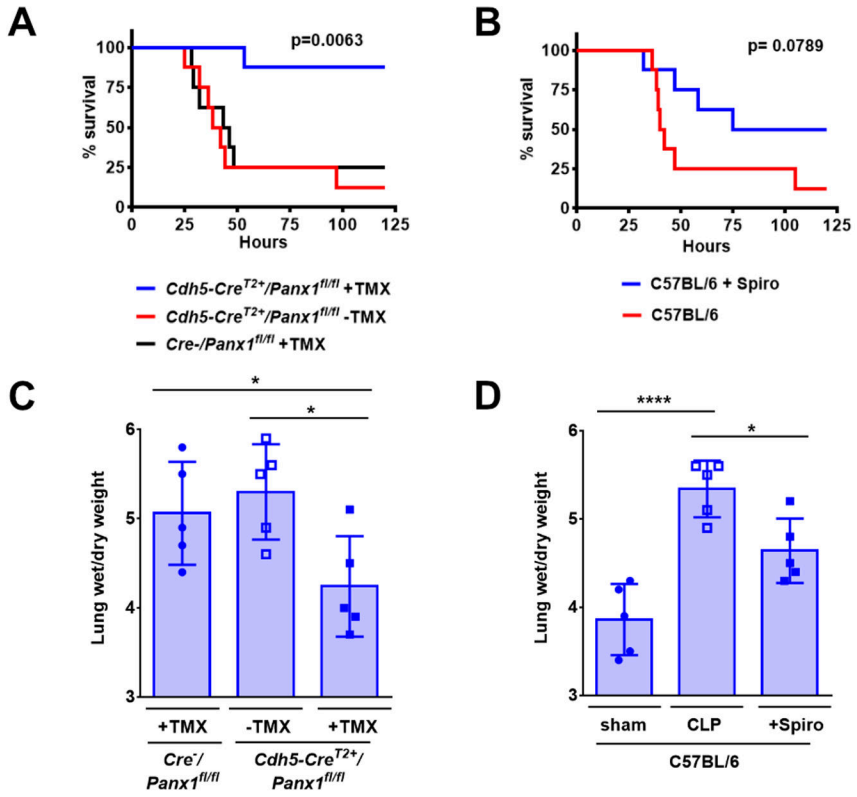

Figure 7. Panx1 inhibition improved survival from systemic sepsis.

(**A,B**) Survival after cecal ligation and puncture (CLP) protocol to induce systemic sepsis was assessed in *Cdh5-CreER*$^{T2+}$*/Panx1*$^{fl/fl}$ mice injected with tamoxifen (+TMX) to induce *Panx1* deletion, non-induced *Cdh5-CreER*$^{T2+}$*/Panx1*$^{fl/fl}$ mice, −TMX-treated *Cre*$^{-}$ mice expressing Panx1 (**A**), or WT C57BL/6 mice treated or not with spironolactone (+Spiro) (**B**). n = 8 mice per group. (**C,D**) 24 h after CLP injury, lungs were isolated and the wet/dry weight ratio was determined as a measure of pulmonary edema in the indicated groups. n = 5 mice per group. Kaplan Meier curves were assessed by Log Rank Mantel-Cox test. (A). * P= 0.038, 0.011 (C), * P = 0.010, **** P < 0.0001 (D), by one-way ANOVA with Fisher's LSD test. Graphs are mean ± SD.

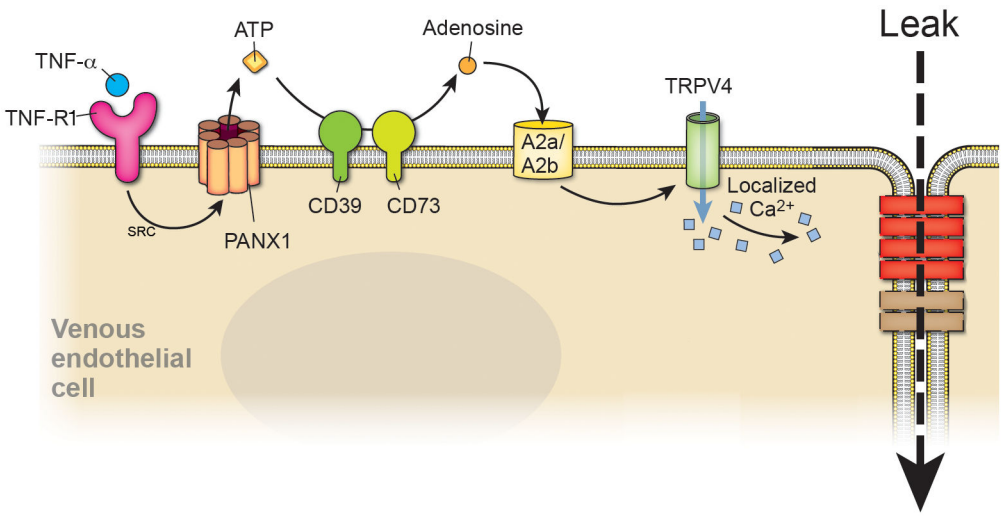

Figure 8. Model depicting the pathway stimulated by TNFα to increase venous endothelial permeability.

TNFα-R1 induces opening of Panx1 channels at the plasma membrane (through SRC) that release ATP from the cytosol to the extracellular environment. ATP is hydrolyzed by CD39 and CD73 to adenosine which then stimulates A_{2A}/A_{2B} receptors. TRPV4 channel are activated, resulting in an increase in paracellular leak through venous tight junction remodeling.